

## The Influence of Anode Composition on the Electrochemical Ferrate (VI) Production in Molten KOH

Lucia Hrnčiariková, Kamil Kerekeš, Ján Híveš, Miroslav Gál\*

Department of Inorganic Technology, Faculty of Chemical and Food Technology, Slovak University of Technology in Bratislava, Radlinského 9, 812 37 Bratislava, Slovakia.

\*E-mail: [miroslav.gal@stuba.sk](mailto:miroslav.gal@stuba.sk)

Received: 25 March 2013 / Accepted: 23 April 2013 / Published: 1 June 2013

---

Cyclic voltammetric and electrochemical impedance spectroscopic analysis were utilized to study a process of electrochemical ferrate(VI) synthesis in the molten potassium hydroxide at three anode materials: pure iron (Fe), white cast iron (FeC) and silicon-rich steel (FeSi) electrodes. Several anodic and corresponding cathodic voltammetric peaks are observed during electrode treatment. The most negative anodic peaks are assigned to Fe(0)→Fe(II) and Fe(II)→Fe(III) reactions and subsequent layer reconstruction and/or transformation. Immediately after passivity region the transpassive iron dissolution, including ferrate(VI) formation together with an oxygen evolution occurs and the current peaks are visible for all electrodes used. This peak is the best developed for Fe electrode. In the case of the FeC electrode, only current shoulder is visible. With increasing temperature the visibility of this peak is getting better for all three electrodes. For all systems linear dependences of the current density on square root of the polarization rate at low polarization rates were found indicating that the electrode reaction kinetic is controlled by the mass transport under the semi-infinite linear diffusion conditions. At higher scan rates current densities decrease indicating that a chemical step becomes rate determining at high polarization rates. Impedance data confirm the physical model of the polarized surface based on the concept of two, inner and outer surface sublayers. For all three electrodes resistances of inner and outer layers decrease with increasing applied potential. With increasing temperature the resistance of inner and outer layer decreases. The capacities of both layers increase with increasing potential, i.e. layers are getting thinner and/or more disintegrated.

---

**Keywords:** Ferrate(VI), Hydroxide melt, Anodic dissolution, Impedance spectroscopy, Electrochemical synthesis

### 1. INTRODUCTION

Electrochemical DC (direct current) and AC (alternating current) techniques were found to be suitable for interfacial and metal dissolution studies in both aqueous and molten environments [1-13]. Active iron dissolution in concentrated alkaline environment has been studied intensively by several

research groups over the years [14-17]. It is well known, that in such solutions iron can be dissolved as ferrous(II), ferric(III) and, finally, ferrate(VI) species depending on the electrode potential and temperature [16]. Transpassive iron dissolution in alkaline solutions is discussed less frequently. Poggendorf [18] observe formation of ferrates(VI) by anodic oxidation of an iron electrode in a concentrated alkaline solution. Haber [19] and Pick [20] using an iron anode have prepared potassium ferrate by electrolyzing concentrated potash solution. They have found that the current yield increased with electrolyte concentration, temperature, as well as with the carbon content in iron electrode [16]. Grube et al. [21] used superimposed alternating current in order to increase a current yield during ferrate(VI) production. The influence of an anode composition on electrochemical ferrate(VI) synthesis was also intensively studied [22-25]. Another important factor that influences the ferrate(VI) production is an electrolyte composition [6]. Pick [20] reported the decrease of the current density from ca. 50% in NaOH to 37% in KOH indicating qualitatively different dissolutions of iron anode. Similar behavior was observed by Bouzek et al. on both iron and white cast iron electrodes [26]. Lapique and Valentine [27] suggested the utilization of mixture NaOH:KOH instead of either pure KOH or NaOH. They wanted to combine high efficiency of ferrate(VI) synthesis in NaOH electrolyte and low solubility of ferrates(VI) in alkaline solutions with the presence of  $K^+$  ions. However, He et al. recently reported the better suitability of KOH electrolyte instead of NaOH as a whole [28]. They found that the current efficiency for KOH was ca. 73% compare to 55% for NaOH. Moreover, the purity and stability was better in the case of KOH than in NaOH solution. Several attempts were also made to describe the reaction mechanism during iron transpassive dissolution [4, 6, 25, 29-38].

The main goal of this work was complex study of a transpassive electrochemical preparation of ferrates(VI) by anodic dissolution of pure iron (Fe), silicon-rich steel (FeSi) and white cast iron (FeC) electrodes in the molten potassium hydroxide (KOH). The great advantage of molten medium to previous aqueous electrolytes is almost water-free environment, high temperature and, therefore, high reaction kinetics and efficiency.

## 2. EXPERIMENTAL

Potassium hydroxide (KOH; p.a., Mikrochem Ltd. Pezinok, Slovakia) was used to prepare molten electrolyte. The real purity of KOH was determined by acidimetric titration with HCl (p.a., Mikrochem Ltd. Pezinok, Slovakia), using Methyl red indicator (p.a., Lachema Neratovice, Czech republic). Carbonates were determined gravimetrically, by precipitation with barium chloride. (p.a., Lachema Neratovice, Czech republic)

An oil thermostat with calibrated sensor, stainless steel box and PTFE crucible with the sample was used for our experiments. Reference connection of thermocouple was immersed in a Dewar flask with ice-water. Measuring connection of thermocouple was immersed into the melt at the same level as electrodes. Electrochemical measurements were performed using AUTOLAB instrument PGSTAT 20 equipped with FRA2 module (ECO Chemie, The Netherlands). A three electrode electrochemical cell was used for all experiments. Working electrodes (WE) were made from: (A) pure iron (Fe) (99.95 wt.% Fe, 0.005 wt.% C, 0.0048 wt.% Ni and 0.0003 wt.% Mn), (B) silicon steel (FeSi) (3.17 wt. % Si,

0.47 wt.% Cu, 0, 23 wt.% Mn, 0.03 wt.% Ni), and (C) white cast iron (FeC) (3.17 wt.% C in the form of Fe<sub>3</sub>C, 0.44 wt.% Mn and 0.036 wt.% Ni). The geometric area of working electrodes varied from 0.2 to 0.7 cm<sup>2</sup>. The same material (pure Fe) was used as the reference electrode (RE). Counter electrode (CE) was made from mild steel (steel class 11). Measurements were carried out in a PTFE crucible containing the melt of 50 g (KOH-KOH.H<sub>2</sub>O). The temperature was varied in the range 110°C to 160°C. Low temperature limit was given by the temperature of eutectic mixture KOH-KOH.H<sub>2</sub>O (100°C; 86.5 wt. % of KOH). Cyclic voltammograms were recorded in the potential range from -0.3 to 1.8 V vs. RE.

Impedance measurements were carried out in the same systems immediately after the measurement of polarization curves. The potential of the working electrode was gradually increased by 25 mV from 1.35 up to 1.75 V vs. RE. In this area, the formation of ferrates(VI) was expected. Frequency range used for the impedance measurements varied from 10 Hz to 100 kHz. Perturbation signal had a sinusoidal shape with amplitude of 5 mV.

### 3. RESULTS AND DISCUSSION

#### 3.1. Cyclic voltammetry

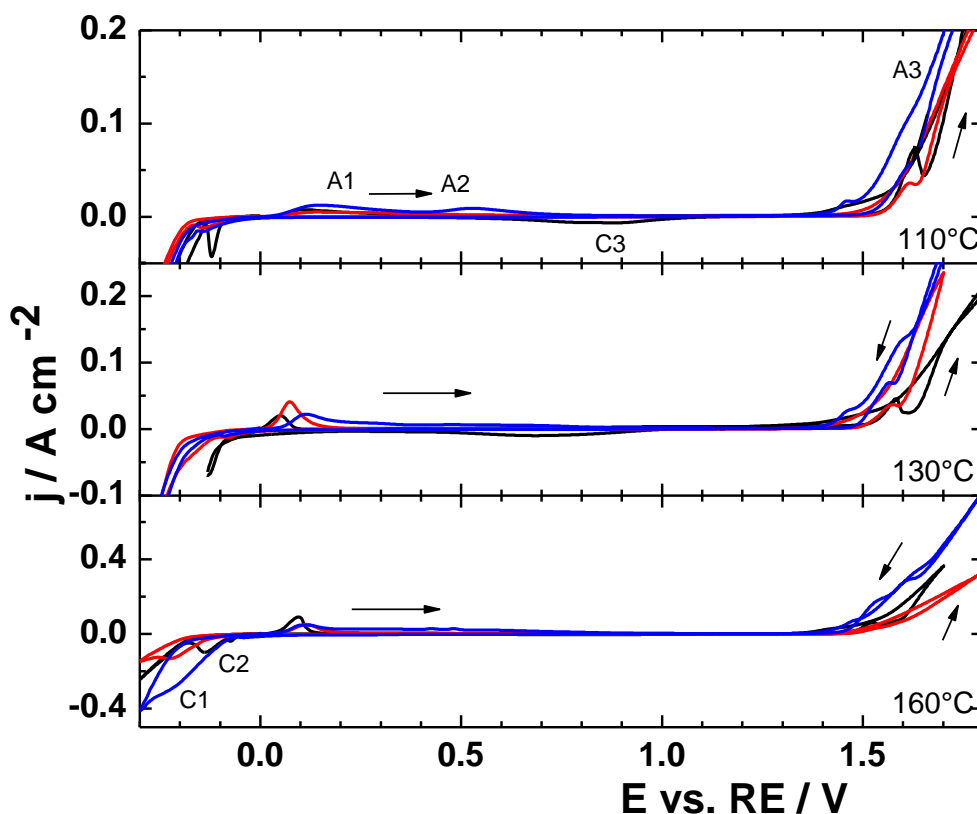


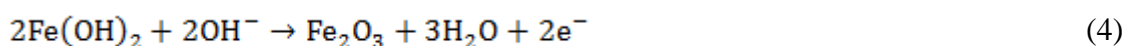
**Figure 1.** Cyclic voltammograms of working electrodes, i.e. pure iron (black line), FeSi (red line), and FeC (blue line) at different temperatures in molten KOH at scan rate of 20 mV s<sup>-1</sup>; temperatures are indicated on the graph; arrows indicate the potential sweep direction.

In Fig. 1 cyclic voltammograms of Fe, FeSi and FeC electrodes in the molten KOH medium at several temperatures are shown. The cathodic part of the potential range is limited by the hydrogen evolution while decomposition of the melt and subsequent oxygen evolution limits anodic one. Oxygen is produced during anodic reaction as well as originates from the reaction of atmospheric oxygen presented in the melt with OH<sup>-</sup> ions [35].

Voltammetric curves are characterized by the presence of several anodic and cathodic current peaks. The intensity of peaks depends on both temperature and electrode materials used. On the anodic part of the cyclic voltammograms at 110°C for FeC electrode two separated current peaks A1 at around 0.15 V vs. RE, and A2 peak are presented. On the other side, the separation of A1 and A2 peaks is worse for FeSi electrode, and for Fe electrode only shoulder following A1 peak can be found. As stated previously [6] the current peak A1 corresponds to the Fe(II) formation:



Subsequent anodic polarization leads to the A2 peak formation (ca 300 mV more positively than A1). The oxidation process can be alternatively described according to the following equations [6]:



It is probable that a part of Fe(OH)<sub>2</sub> layer reacts with the environment forming  $\text{FeO}_2^{2-}$ . However, the exact mechanism is not known and, unfortunately, it is not detectable in situ at the electrochemical conditions. It must be noted that one can hardly expect complete stoichiometric oxidation of the hydroxidic layer. In agreement with previous observations the formation of the layer composed of nonstoichiometric species similar to the magnetite with better protecting properties is more probable [25]. At high temperatures (160°C) for all three electrodes only one, well developed, A1 peak followed by shoulder, A2 peak, is visible. Probably due to the kinetic limitation of overall process and specific insulating properties of the surface layer current peak A2 is less visible in the case of FeSi and pure iron electrodes than A1 one at low temperatures and for all electrodes at high temperatures [6]. The highest current density for A1 and A2 peak are found for FeC electrode and the lowest for iron electrode. However, the differences are not as high as reported by Macova et al. [23-25, 39] in high alkaline aqueous solutions. Therefore, it may be summarized that the structure of the anode positively influences the ability of the Fe species to form corresponding oxo/hydroxy layers. After the remarkable decrease of the current densities for all three electrodes due to their passivation, new broad, not perfectly pronounced current peak in the region 1.1-1.25 V vs. RE is observed. This peak, as stated before, is assigned to the transformation and restructuring of an anodic solid surface layer [25]. Subsequently, after passivity region the transpassive anodic electrode dissolution, including ferrate(VI) formation followed by oxygen evolution occurs and new A3 current peak at about 1.6 V vs. RE is

formed. Only slight differences in the A3 peak potentials are observed among electrodes. This peak is the best developed for the pure iron electrode. In the case of the FeC electrode, only current shoulder is visible. With increasing temperature the visibility of A3 peak is getting better for all three electrodes. It must be noted that for all electrode materials the hysteresis in the course of voltammetric curve in the transpassive potential region was observed. It is probably caused by the reduction of the inhibition properties of the surface layers because of their dissolution at high potentials and due to the oxygen evolution causing the mechanical disruption of the anode surface. At higher temperatures the peak potential of A3 peak is slightly shifted to the more negative potentials indicating the lower energy demand for oxidation process. This feature is probably caused also by the disrupted oxo-hydroxide surface film.

In the opposite cathodic direction three peaks corresponding to three anodic peaks appeared. A broad reduction peak of ferrate(VI) (peak C3) occurs at potentials of 0.6 to 0.80 V vs. RE depending on both temperature and electrode material used. This peak C3 is, at all temperatures, best pronounced for Fe electrode. For both FeSi and FeC electrodes only low, broad peak is observed. In the case of FeC electrode low cathodic current peak at 1.25 V is also visible. With increasing the temperature the peak of ferrates(VI) reduction (peak C3) is slightly shifted to the more positive potentials indicating less energy requirement for their reduction.

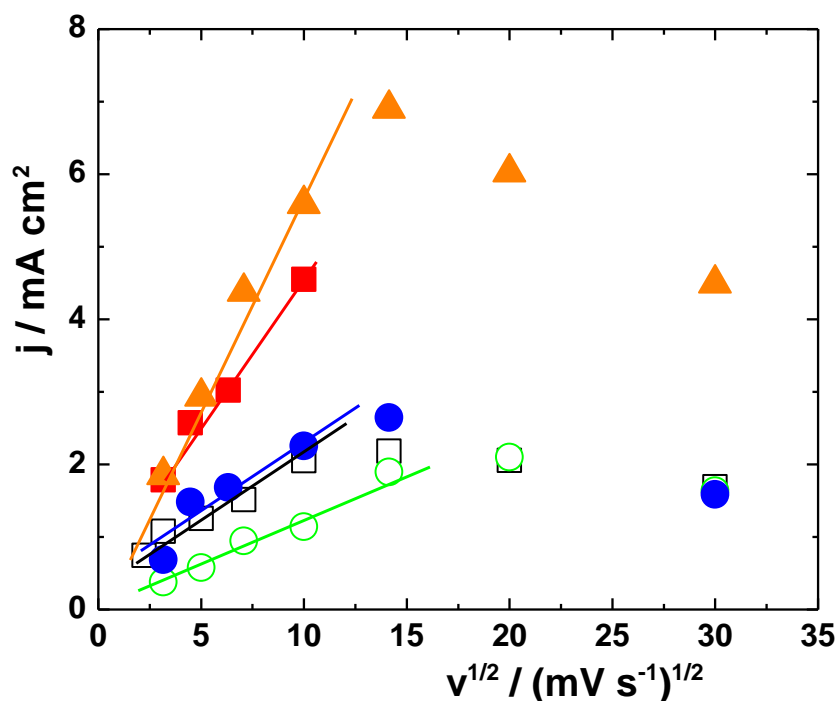


**Figure 2.** The dependences of the anodic peak current densities (A3) on the square root of potential scan rate; □ pure Fe electrode at 110°C; ■ pure Fe electrode at 160°C; ○ FeSi electrode at 110°C; ● FeSi electrode at 160°C; ▲ FeC electrode at 160°C.

This probably indicates that the collapse of compactness of anode passive layer occurred. It is important finding with respect to possible increase of anode efficiency of ferrate(VI) formation. In the case of peak C3 the highest current densities are observed for pure iron electrode. The current densities corresponding to the in the region of ferrate(VI) reduction is very low. This signifies that the amount

of ferrates(VI) undergoing reduction in this potential region is the highest for pure iron electrode. At the potential region 0 V to -0.25 V vs. RE peaks that correspond to the reduction of Fe(III) to Fe(II) (peak C2) and subsequent reduction to Fe(0) (peak C1) are found. Both are shifted to the more negative potentials with increasing temperature for all electrodes. One can therefore conclude, that the structure of the anode layers plays an important role in ferrate(VI) production also in molten salts environment similarly to strong alkaline aqueous ones [23-25].

In the next Fig. 2 the dependences of the A3 peak current density on the square root of potential scan rate for both various materials and temperatures are plotted.

For all systems the linear dependences of the current density on square root of the polarization rate in the region below  $0.2 \text{ V s}^{-1}$  were found indicating that the electrode reaction kinetic is controlled by the mass transport under the semi-infinite linear diffusion conditions [25]. At higher scan rates current densities after reaching a certain maximum at about  $250 \text{ mV s}^{-1}$  decrease with further increasing of the polarization rate. It seems, that some chemical step due to the electrode structure become rate determining when scan rate reach ca.  $250 \text{ mV s}^{-1}$ . Our observation is in agreement with some previous results in the hydroxide melts [35]. In the strong alkaline aqueous solutions the subsequent chemical reaction was also observed [23-25].

### 3.2. Electrochemical impedance spectroscopy

EIS was used to deeply characterize ferrate(VI) production because this method is suitable for properties and surface layer structure studies. Nyquist plots of impedance data obtained for FeSi electrode at several potentials are shown in Fig. 3.

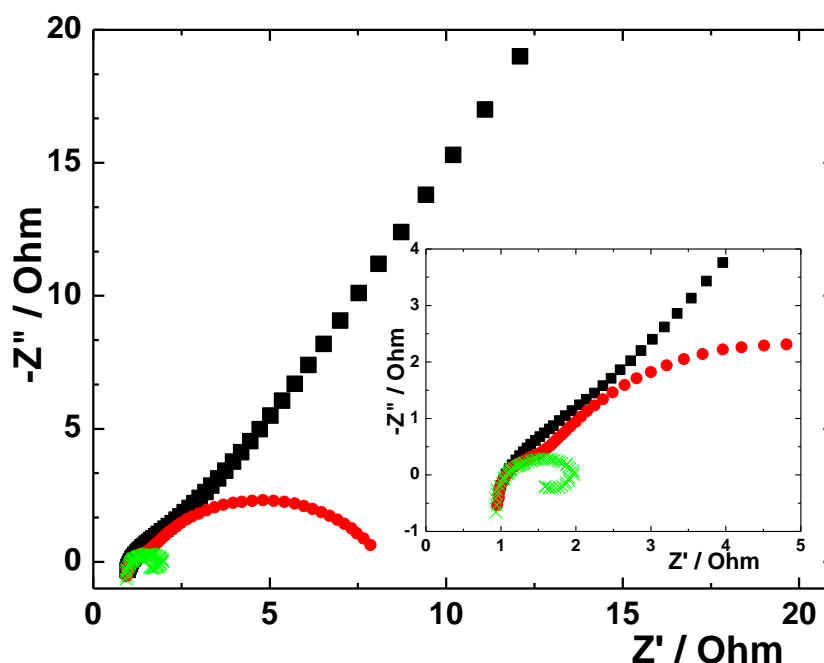


**Figure 3.** Nyquist plots of impedance spectra for FeSi electrode at  $t = 120^\circ\text{C}$  and at chosen anodic potentials vs. RE: ■ 1.45 V; ● 1.55 V; × 1.65 V.

Nyquist plots in Fig. 3 show two time constants indicating that at least two processes influence ferrates(VI) formation. To characterize this processes the electrochemical behavior of electrodes in molten KOH was represented by an equivalent circuit. (see Fig. 4) The proposed model is based on the concept of two macrohomogeneous surface layers [25]. Two parallel R-Q (constant phase element) impedance elements characterizing individual layers (inner, outer) connected in series together with one resistant ( $R_s$ ) and one inductance ( $L$ ) element compose the simplest equivalent circuits that fit our experimental data with acceptably low  $\chi^2$ . Constant phase element (Q) was used instead of pure capacitance element (C) to underline the nonlinearity of the ferrate(VI) production process. Similar approaches were utilized in mixed NaOH-KOH medium and in strong alkaline aqueous medium [23-25, 36].

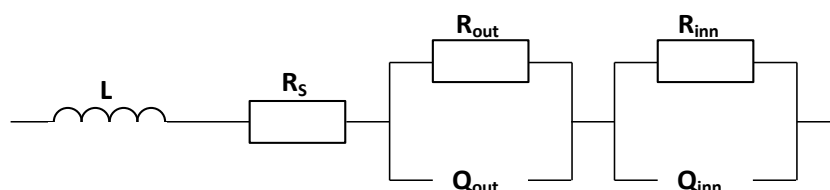


**Figure 4.** Equivalent circuit representing the impedance of the system containing electrode and KOH melt;  $R_s$ , electrolyte resistance;  $L$  outer inductance;  $R_{in/out}$ , inner/outer layer resistance;  $Q_{in/out}$ , inner/outer layer constant phase element.

The accuracy of proposed equivalent circuit is documented on Bode plot (Fig. 5) where lines represent the results of the nonlinear regression analysis according to the model in Fig. 4.

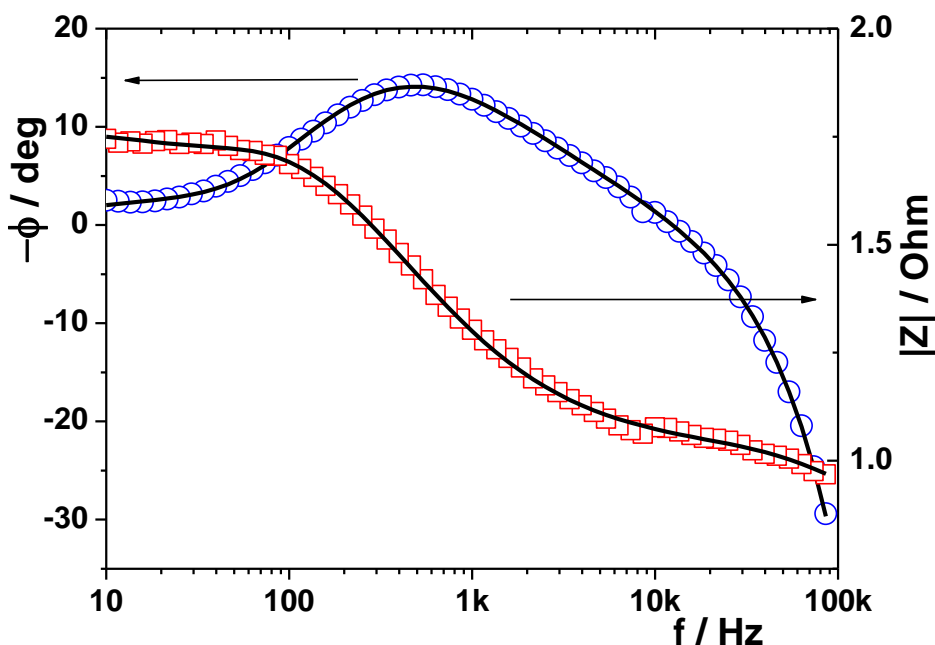


**Figure 5.** Bode plot. FeSi electrode;  $t = 150^\circ\text{C}$ ;  $E_{\text{anodic}} = 1.65 \text{ V vs. RE}$ . Points represent experimental data, curves nonlinear regression analysis according to proposed equivalent circuits (Fig. 4).

The optimized parameters of nonlinear analysis of the equivalent circuit for white cast iron (FeC) electrode at low and high temperatures in dependence on the electrode potential are shown in Fig. 6.

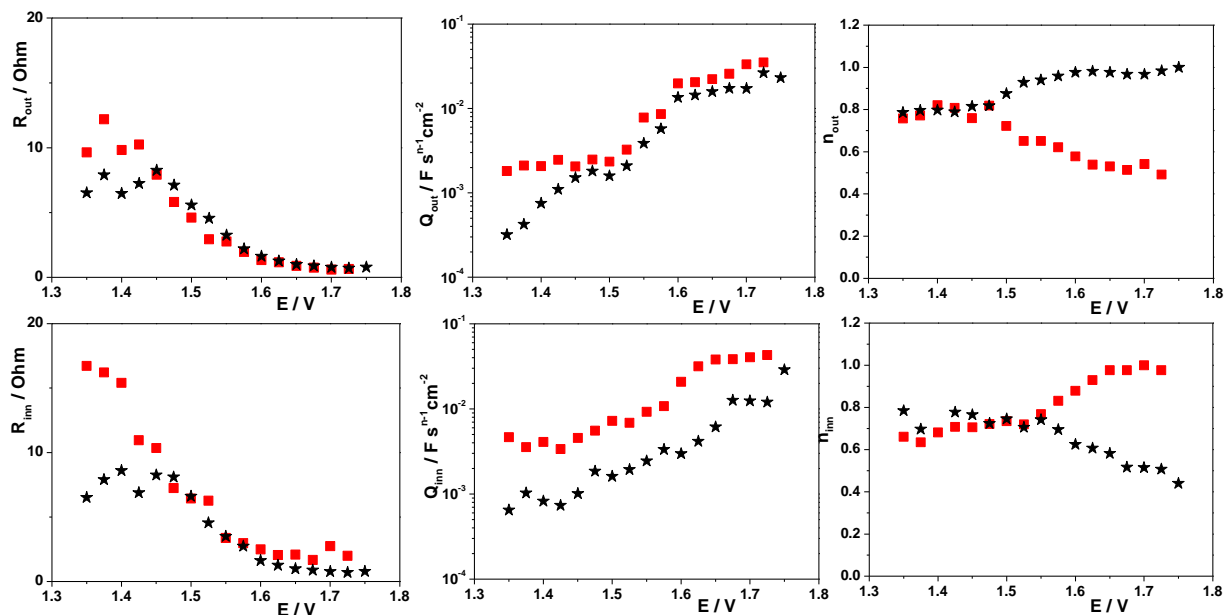


**Figure 6.** The fitted values of the equivalent circuit elements obtained for both inner and outer layer in dependence on the polarization potential of the FeC electrode at various temperatures: ■ 120°C; \* 160°C.

From Fig. 6 it can be seen that resistances of both inner and outer layer decrease with increasing applied potential. This means that either both layers are getting thinner with increasing potential or are disintegrated by strong anodic potential or by strong oxygen evolution. Resistances of both outer and inner layer are approximately equal indicating the same thickness or compactness. With increasing temperature the resistances of the layers slightly decreases. This means that the charge is at higher temperatures easily transferred; the layer is either thinner or less compact. At about 130°C the resistances are almost equal for individual sublayers. Moreover, three regions are visible in these plots: short plateau at the beginning indicating stability of the individual layers at the end of the passivity region, then relatively fast decrease of the resistance of both layers meaning either reduction of the thickness or the development of the spongy or porous structures in the both layers, and at the end of measured potential second plateau that can be assigned to disrupted layers. Similar behavior was found in the case of both strong alkaline aqueous solutions and mixed NaOH-KOH molten solutions [23-25, 36]. However, resistances of both sublayers (especially inner one) are lower than in alkaline aqueous solutions meaning either individual layers are thinner or more disintegrated in molten medium due to the higher temperature and/or more aggressive environment [23-25]. The capacity of inner and outer layer increases with increasing potential. This is in agreement with decrease of the resistances of both layers: layers are getting thinner or more disintegrated by oxygen evolution and/or strong anodic dissolution. Capacities of inner and outer layers are almost independent of the

temperature meaning that both layers are losing their thickness or compactness approximately equally at all the temperature used. The same behavior is observed in mixed NaOH-KOH molten solution [36]. Contrary, in alkaline aqueous solutions [23-25] higher capacities of both individual layers that depend on a temperature of the system are found. The highest dependence is found for pure Fe electrode [23-25]. This is in good agreement with observations concerning resistances measurements.

From  $n$  parameter of the constant phase element supplementary information characterizing the surface structure of the electrode can be obtained. Similarly to the resistances, the curve of the dependence of  $n_{\text{out}}$  on  $E$  can be divided into three regions for both layers indicating the same changes in both individual layers with increasing potentials. The outer layer at lower temperature is getting porous or spongy and, vice versa, at higher temperatures becomes more ideal with increasing polarization potential. Bearing in mind the previous conclusions about  $R_{\text{out}}$  and  $Q_{\text{out}}$ , one should think about the disintegration of the outer layer rather than reduction in its thickness. In the case of mixed molten medium no dependence of  $n_{\text{out}}$  on  $E$  was found [36]. In alkaline aqueous solutions no differences are found among solutions temperatures: either almost monotonous grow or decrease of  $n_{\text{out}}$  vs.  $E$  is observed for all electrodes and at all temperatures used [23-25].

Contrary to previous observations,  $n_{\text{inn}}$  changes from quasi ideal to spongy at high temperature and to ideal at lower temperatures. Therefore, the conclusions made for  $R_{\text{inn}}$  and  $Q_{\text{inn}}$  are connected to the reduction in thickness of the inner layer rather than its disintegration especially at low temperatures. The stability of both layers seems to be equal depending on the temperature. One can conclude that temperature has an impact on the thickness of the individual layers, but not on their compactness. This tendency was also observed in mixed molten solution [36].

Parameters for other two electrodes show the similar trends as in the case of FeC one (not shown). However, there are some differences among them:  $R_{\text{inn}}$  and  $R_{\text{out}}$  are the highest for pure iron electrode and slightly higher for FeSi than for FeC electrode. These differences are not as high as in aqueous alkaline solutions [23-25]. The capacities of individual layers are the highest for FeC electrode and the lowest for pure Fe electrode. Both parameters indicate that the layers are the thickest for pure iron electrode and the thinnest for FeC electrode. This statement corresponds with CV results, where C3 peak was the highest for pure iron electrode meaning the highest amount of ferrate(VI) presented on the electrode surface.

#### 4. CONCLUSIONS

A process of electrochemical ferrate(VI) production in molten potassium hydroxide at three different anode materials, i.e. pure iron (Fe), white cast iron (FeC) and silicon-rich steel (FeSi) electrodes was studied by cyclic voltammetry and electrochemical impedance spectroscopy techniques. Several anodic and cathodic voltammetric peaks were observed during electrode treatment. The most negative anodic peaks are assigned to  $\text{Fe}(0) \rightarrow \text{Fe}(\text{II})$  and  $\text{Fe}(\text{II}) \rightarrow \text{Fe}(\text{III})$  reactions and subsequent layer reconstruction and/or transformation. After passivity region the transpassive iron dissolution, including ferrate(VI) formation together with an massive oxygen evolution occurs. The corresponding current peaks of ferrate(VI) production are visible for all electrodes used. This peak is the best developed for

Fe electrode. On the other hand, only current shoulder is visible in the case of the FeC electrode. With increasing temperature the visibility of this peak is getting better for all three electrodes. Linear dependences of the current density on square root of the polarization rate at low polarization rates were found indicating that the electrode reaction kinetic is controlled by the mass transport under the semi-infinite linear diffusion conditions. At higher scan rates current densities decrease indicating that a chemical step becomes rate determining at high polarization rates. Impedance data confirm the physical model of the polarized surface based on the concept of two, inner and outer surface sublayers. For all three electrodes resistances of inner and outer layers decrease with increasing applied potential. With increasing temperature the resistance of inner and outer layer decreases. The capacities of both layers increase with increasing potential, i.e. layers are getting thinner and/or more disintegrated.

#### ACKNOWLEDGEMENTS

The authors gratefully acknowledge the financial support for this research by the Ministry of Education, Science, Research and Sport of the Slovak Republic within project VEGA 1/0985/12 and by the Research & Development Operational Programme funded by the ERDF within project ITMS 26240220073.

#### References

1. C. Cuevas Arteaga, *Int. J. Electrochem. Sci.* 7 (2012) 12283
2. T.-J. Kim, B. O. Jeong, E. H. Lee, D.-H. Ahn, Y. Jung and S.-W. Paek, *Int. J. Electrochem. Sci.* 7 (2012) 11257
3. J. L. Trinstancho-Reyes, M. Sanchez-Carrillo, R. Sandoval-Jabalera, V. M. Orozco-Carmona, F. Almeraya-Calderon, J. G. Chacon-Nava, J. G. Gonzalez-Rodriguez and A. Martinez-Villafane, *Int. J. Electrochem. Sci.* 6 (2011) 419
4. K. Bouzek, M. Lipovská, M. Schmidt, I. Roušar and A. A. Wragg, *Electrochim. Acta* 44 (1998) 547
5. J. J. Dyrtrtova, M. Jakl, D. Schroder and T. Navratil, *Curr. Org. Chem.* 15 (2011) 2970
6. J. Hives, M. Benova, K. Bouzek, J. Sitek and V. K. Sharma, *Electrochim. Acta* 54 (2008) 203
7. M. Naumowicz, A. D. Petelska and Z. A. Figaszewski, *Electrochim. Acta* 54 (2009) 1089
8. M. Naumowicz, A. D. Petelska and Z. A. Figaszewski, *Cell Biochem. Biophys.* 61 (2011) 145
9. M. Naumowicz, A. D. Petelska and Z. A. Figaszewski, *Steroids* 76 (2011) 967
10. L. Novotny, T. Navratil, S. Sander and P. Basova, *Electroanalysis* 14 (2002) 1105
11. L. Novotny, T. Navratil, S. Sander and P. Basova, *Electroanalysis* 15 (2003) 1687
12. A. D. Petelska, M. Naumowicz and Z. A. Figaszewski, *Langmuir* 28 (2012) 13331
13. I. Sestakova and T. Navratil, *Bioinorg. Chem. Appl.* 3 (2005) 43
14. R. D. Armstrong and I. Baurhoo, *J. Electroanal. Chem.* 40 (1972) 325
15. D. D. MacDonald and B. Roberts, *Electrochim. Acta* 23 (1978) 781
16. I. Serebrennikova, I. Paramasivam, P. Roy, W. Wei, S. Virtanen and P. Schmuki, *Electrochim. Acta* 54 (2009) 5216
17. H. Zhang and S.-M. Park, *J. Electrochem. Soc.* 141 (1994) 718
18. J. C. Poggendorf, *Pogg. Ann.* 54 (1841)
19. F. Haber, *Z. Elektrochem.* 7 (1900) 215
20. W. Pick, *Z. Elektrochem.* 7 (1901) 713
21. G. Grube and H. Gmelin, *Z. Elektrochem. Angew. P.* 26 (1920) 153
22. A. Denvir and D. Pletcher, *J. Appl. Electrochem.* 26 (1996) 823
23. Z. Macova and K. Bouzek, *J. Appl. Electrochem.* 41 (2011) 1125

24. Z. Macova and K. Bouzek, *J. Appl. Electrochem.* 42 (2012) 615
25. Z. Macova, K. Bouzek and V. K. Sharma, *J. Appl. Electrochem.* 40 (2010) 1019
26. K. Bouzek, M. J. Schmidt and A. A. Wragg, *Electrochem. Commun.* 1 (1999) 370
27. F. Lapique and G. Valentin, *Electrochem. Commun.* 4 (2002) 764
28. W. C. He, J. M. Wang, H. B. Shao, J. Q. Zhang and C. N. Cao, *Electrochem. Commun.* 7 (2005) 607
29. F. Beck, R. Kaus and M. Oberst, *Electrochim. Acta* 30 (1985) 173
30. K. Bouzek, L. Flower, I. Roušar and A. A. Wragg, *J. Appl. Electrochem.* 29 (1999) 569
31. K. Bouzek and I. Roušar, *J. Appl. Electrochem.* 23 (1993) 1317
32. K. Bouzek, I. Roušar, H. Bergmann and K. Hertwig, *J. Electroanal. Chem.* 425 (1997) 125
33. M. De Koninck and D. Bélanger, *Electrochim. Acta* 48 (2003) 1435
34. M. De Koninck, T. Brousse and D. Bélanger, *Electrochim. Acta* 48 (2003) 1425
35. J. Hives, M. Benova, K. Bouzek and V. K. Sharma, *Electrochem. Commun.* 8 (2006) 1737
36. J. Hives, Z. Macova, M. Benova and K. Bouzek, *J. Electrochem. Soc.* 155 (2008) E113
37. J. Toušek, *Collect. Czech. Chem. Commun.* 27 (1962) 914
38. A. S. Venkatadri, H. H. Bauer and W. F. Wagner, *J. Electrochem. Soc.* 121 (1974) 249
39. Z. Macova, K. Bouzek, J. Hives, V. K. Sharma, R. J. Terryn and J. C. Baum, *Electrochim. Acta* 54 (2009) 2673